Global Thermohaline Circulation. Part I: Sensitivity to Atmospheric Moisture Transport

XIAOLI WANG, PETER H. STONE, AND JOCHEM MAROTZKE

Center for Global Change Science, Massachusetts Institute of Technology, Cambridge, Massachusetts

(Manuscript received 15 July 1997, in final form 1 January 1998)

ABSTRACT

A global ocean general circulation model of idealized geometry, combined with an atmospheric model based on observed transports of heat, momentum, and moisture, is used to explore the sensitivity of the global conveyor belt circulation to the surface freshwater fluxes, in particular the effects of meridional atmospheric moisture transports. The numerical results indicate that the *equilibrium* strength of the North Atlantic Deep Water (NADW) formation increases as the global freshwater transports increase. However, the global deep water formation—that is, the sum of the NADW and the Southern Ocean Deep Water formation rates—is relatively insensitive to changes of the freshwater flux.

Perturbations to the meridional moisture transports of each hemisphere identify equatorially asymmetric effects of the freshwater fluxes. The results are consistent with box model results that the equilibrium NADW formation is primarily controlled by the magnitude of the Southern Hemisphere freshwater flux. However, the results show that the Northern Hemisphere freshwater flux has a strong impact on the *transient* behavior of the North Atlantic overturning. Increasing this flux leads to a collapse of the conveyor belt circulation, but the collapse is delayed if the Southern Hemisphere flux also increases. The perturbation experiments also illustrate that the rapidity of collapse is affected by random fluctuations in the wind stress field.

1. Introduction

Freshwater flux is an important component of the buoyancy forces driving the thermohaline circulation. Paleoclimate evidence has raised the possibility of abrupt change of the thermohaline circulation in response to the release of large amounts of meltwater from continental ice sheets (Broecker et al. 1988). In addition, Manabe and Stouffer (1994) have shown with a coupled ocean–atmosphere general circulation model that, when the atmospheric CO_2 was gradually increased with time, the thermohaline circulation was weakened significantly, which was attributed to the enhanced poleward atmospheric moisture transport in the warmer model troposphere.

The sensitivity of the thermohaline circulation to changes of the surface freshwater fluxes, both in spatial distribution and intensity, has been extensively studied in many ocean climate studies (Weaver et al. 1991, 1993; Winton and Sarachik 1993; Huang and Chou 1994; Chen and Ghil 1995). All these studies used idealized ocean general circulation models (OGCMs) of one hemisphere only. However, there is strong evidence that the Atlantic thermohaline circulation is actually governed by pole-to-pole overturning dynamics. For example, Hughes and Weaver (1994) found that the intensity of the thermohaline circulation in the North Atlantic is linearly related to the zonally and vertically averaged steric height difference between the northern high-latitude sinking region and the tip of Africa. Similarly, Rahmstorf (1996) identified a linear relation between the North Atlantic Deep Water (NADW) formation rate and interhemispheric density differences at middepth. Klinger and Marotzke (1999) found that strong equatorially asymmetric thermohaline circulation was generated in a temperature-only model when restoring temperatures were weakly different in the two polar regions. These results point to the importance of the pole-to-pole dynamics of the thermohaline circulation in the Atlantic and therefore raise the possibility that the results obtained with single-hemispheric ocean models may be incomplete or even distorted.

Here, we investigate the sensitivity of the global thermohaline circulation to changes of the global freshwater fluxes. In particular, we want to assess the effects of equatorially asymmetric perturbations in the atmospheric moisture transports. Apart from the global perspective, an important difference here from earlier studies is that our oceanic freshwater flux forcing is directly determined by observed meridional atmospheric moisture transports. Sensitivity experiments are performed

Corresponding author address: Jochem Marotzke, Room 54-1514, MIT, 77 Massachusetts Ave., Cambridge, MA 02139.
E-mail: jochem@sound.mit.edu

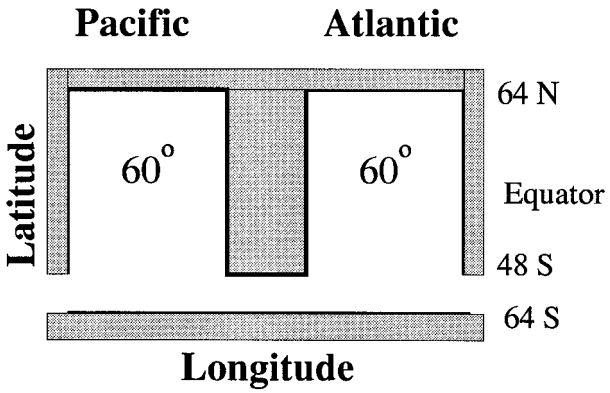

FIG. 1. Geometry of the global ocean model.

by slowly increasing these transports, in each hemisphere separately and jointly. Both the equilibrium and the transient responses of the thermohaline circulation to such surface freshwater flux perturbations are investigated.

To this end, we employ an idealized global OGCM, with the same model geometry as in Marotzke and Willebrand (1991, hereinafter MW91). Mixed boundary conditions are used (restoring conditions on surface temperature, prescribed freshwater flux), but the specification of the restoring time and the target temperature profile are derived from a simplified atmospheric model, where the atmospheric heat transport and the radiative forcing are specified from observations. This approach is equivalent to damping SST anomalies through longwave radiative relaxation (Schopf 1983; Zhang et al. 1993). The advantage of this approach is that it can be readily extended to a fully coupled hybrid model. Results obtained with the coupled model will be presented in Part II (Wang et al. 1998).

This paper is organized as follows. In section 2, the OGCM is briefly described, along with the derivation of the mixed boundary conditions based on the observed atmospheric transports. In section 3, the conveyor belt circulation of the control run is presented, as well as the equilibrium responses of the thermohaline circulation to changes of the atmospheric moisture transports. In section 4, a series of sensitivity experiments for the transient responses of the thermohaline circulation to equatorially asymmetric atmospheric moisture transports are discussed. A summary and conclusion follow in section 5.

2. Model description

a. Oceanic model

The OGCM used in this study is the Geophysical Fluid Dynamics Laboratory (GFDL) Modular Ocean Model [MOM 1.1, Pacanowski et al. (1991)]. The model setup is, in most aspects, identical to that of MW91 (Fig. 1), thus facilitating comparisons with their results. The model consists of two identical basins, each of 60° width. The ocean domain extends from 64°N to 64°S. A channel representing the Antarctic Circumpolar Current (ACC) connects the two basins from 48°S to 64°S. From several experiments performed with various horizontal resolutions (e.g., $2° \times 2°$ vs $4° \times 4°$), Weaver et al. (1993) concluded that, within the context of coarse-resolution modeling, the exact nature of the coarse resolution is not important in determining the stability and variability properties of the thermohaline circulation. Therefore, coarse horizontal resolutions of 3.75° long and 4° lat were chosen for this study, the same as in MW91. There are 15 levels in the vertical, with intervals varying from 50 m near the surface to 500 m near the bottom. The bottom is taken to be flat, and has uniform depth of 4500 m.

The mass transport in the ACC is difficult to represent in a coarse-resolution model with flat bottom. Following MW91, the ACC transport is thus prescribed, and a value of 140 Sv (Sv $\equiv 10^6$ m^3 s^{-1}) is used. Since the wind stress forcing of the ACC is held fixed in all our experiments, the fixed strength of the ACC is appropriate here. The sole role of the ACC in our experiments is that it provides a connection between the two basins. The two basins are identical in geometry and can arbitrarily be referred to as Pacific or Atlantic. Constant mixing coefficients are used. To ensure numerical stability, the horizontal viscosity A_H must be large enough to allow the viscous western boundary layer to be resolved (Bryan et al. 1975), and it is taken as 2.5×10^5 m^2 s^{-1}, the same value as in MW91. The diffusivities follow MW91, with horizontal and vertical diffusivities of $K_H = 10^3$ m^2 s^{-1}, and $K_v = 5 \times 10^{-5}$ m^2 s^{-1}. For the vertical viscosity we choose $A_v = 10^{-2}$ m^2 s^{-1}, two orders of magnitude higher than in MW91, in order to suppress inertial instability near the equator (Weaver and Sarachik 1990).

Since the evolution of momentum is much faster than that of tracers (temperature and salinity), Bryan (1984) suggested that the time steps for momentum and tracers be split to accelerate the integration to equilibrium, a technique called asynchronous integration. The asynchronous integration is used during all our experiments, with a time step of 2 h for momentum and 2 days for tracers. To prevent leapfrog time splitting, there is mixing between time steps every 17 time steps. As Bryan (1984) showed, long baroclinic Rossby waves, which affect the adjustment of the interior density field, are unaffected by this acceleration technique; hence it is applicable to our transient experiments.

The convection scheme was provided to us by Yin and Sarachik (1994). It completely removes all static instability at each time step. The rigid-lid approximation ($w = 0$ at $z = 0$) is used at the surface, a free-slip condition ($\partial \mathbf{V}/\partial z = 0$) at the bottom, and a no-slip condition ($\mathbf{V} = 0$) at the lateral walls. There is no heat or salt flux at the bottom and the lateral walls.

b. Atmospheric model

Our atmospheric model has no explicit representation of the atmosphere's momentum budget. Instead a zonally uniform annual mean wind stress, identical to that used by MW91, is prescribed as a function of latitude only. This wind stress, although idealized, reflects the major features of the observed distribution.

The atmospheric budgets of heat and moisture assume that the atmospheric heat and moisture capacities are zero. Thus, the surface oceanic heat flux is determined by the divergences of atmospheric heat transport and net radiative forcing at the top of the atmosphere. The net radiative forcing at the top of the atmosphere is expressed as

$$R = Q(1 - \alpha) - I, \tag{1}$$

where Q is the incoming solar radiation, α is the planetary albedo, and I is the outgoing longwave radiation. Both Q and α are specified from annual mean observations, and are approximated by Legendre polynomials, symmetric about the equator (North 1975; Stephens et al. 1981). Here Q and α are assumed to be fixed, that is, there is no albedo feedback in our model. The longwave radiation follows the empirical relation of Budyko (1969),

$$I = F_0 + \frac{dF_t}{dT_s}T_s, \tag{2}$$

where T_s is the surface temperature (in units of degrees Celsius). Earth Radiation Budget Experiment (ERBE) longwave radiation data (Trenberth and Solomon 1994) and the observed sea surface temperature (SST; Levitus 1982) are used to determine the coefficients F_0 and dF_t/dT_s,

$$F_0 = 195 \text{ W m}^{-2}; \tag{3}$$

$$\frac{dF_t}{dT_s} = 2.78 \text{ W m}^{-2} (^\circ\text{C})^{-1}. \tag{4}$$

In this paper we fix the atmospheric transports, based on observations. Thus, as in Zhang et al. (1993), SST perturbations relax with a timescale determined by the longwave radiation parameterization. However, unlike Zhang et al., our model's fluxes are directly constrained by the observed atmospheric state. Our rationale is that, if the ocean model were spun up under surface forcings directly derived from an observation-based atmospheric model, the coupled model would be likely to avoid artificial flux adjustments later on (see detailed discussion in Part II).

The annual-mean atmospheric meridional heat transport we use, H_d, is based on two datasets, one from rawinsonde data (Oort 1983), the other from ECMWF operational analysis products (Keith 1995). To eliminate any north–south asymmetry in the atmospheric forcing of the ocean, we average the magnitude of the meridional heat transports in the Northern and Southern Hemispheres in the two analyses, and fit the resulting profiles by a series of Legendre polynomials antisymmetric about the equator. The model's H_d is then taken to be the average of the results from the two analyses, as illustrated in Fig. 2. Note that H_d is the total heat flux, not the flux per unit area. There is no explicit zonal heat flux in our atmospheric model.

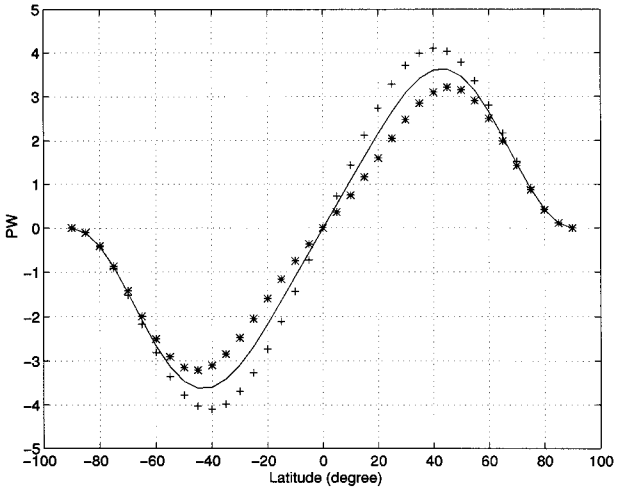

FIG. 2. Annual-mean atmospheric meridional heat transport as a function of latitude, made antisymmetric by averaging the magnitudes of the transport in the Northern and Southern Hemispheres: from Oort (1983, asterisks), from Keith (1995, crosses), and the average, H_d, used in this study (solid curve.)

To estimate the oceanic surface fluxes of heat and freshwater, land has to be considered. The heat capacity of land is assumed negligible, therefore, the surface heat flux over land is zero. Thus the whole imbalance between R and the divergence of H_d is taken up by the surface flux of heat into the ocean. Since in our geometry the oceans occupy one-third of a latitude circle (except in the ACC), this means that the surface flux per unit area into the ocean is three times the zonal-mean surface heat flux per unit area needed to balance the atmospheric heat and radiation fluxes (except in the ACC). Further, the zonal-mean land surface temperature is assumed equal to the zonally averaged SST. Note however that the longwave radiation term I is allowed to differ for each ocean basin, if they have different temperatures, according to Eq. (2).

With the above assumptions, the surface heat flux into the ocean is a linear function of T_s, just as in conventional mixed boundary conditions. The restoring time is determined by the longwave radiative coefficient and the ratio of ocean area to global area (see Marotzke and Stone 1995); in our model this yields a restoring time of 288 days for a top ocean layer 50 m thick. However, in our model the small-scale zonal SST anomalies are removed by zonally averaging the SST within each basin at every time step (2 days). Conceptually, this implies very large zonal mixing efficiency in the atmosphere. This assumption is more realistic than the opposite ex-

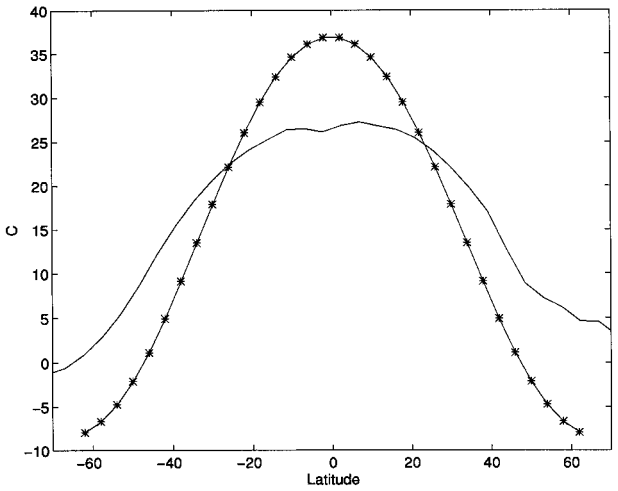

FIG. 3. The Levitus (1982) zonal-mean SST (solid), and the T^* implied by the model (starred), unit: °C.

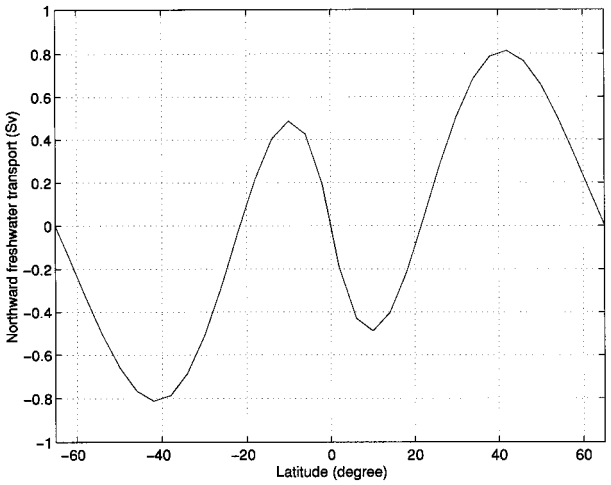

FIG. 4. Zonally integrated annual-mean atmospheric meridional freshwater transport F_w, in Sv, based on observations.

treme, no zonal mixing, which causes the NADW formation in our model to be located in the midlatitudes, rather than near the northern boundary, because the small-scale heat flux anomalies in the surface shift the deep convection locations. Because of the zonal averaging of SST, the zonal average surface heat flux is in effect parameterized by adding to the temperature equation in the surface layer a zonal-mean tendency equal to $0.402 \times 10^{-7}\ \mathrm{s}^{-1}$ [$T^* - T$ (zonally averaged)] in each basin.

The target temperature, T^*, which enters the conventional heat flux boundary condition (Haney 1971) is defined as the equilibrium temperature that the surface atmosphere and ocean would reach in the absence of ocean currents. Our atmospheric model implies a zonally uniform T^*, which we can calculate using our specified atmospheric heat transport and the net radiative forcing parameterization, while setting oceanic heat transport to zero. Figure 3 plots this T^* as a function of latitude. Compared to the observed zonal-mean SST (Levitus 1982), T^* exhibits a much steeper meridional gradient.

The atmospheric meridional moisture transport in our model is based on Baumgartner and Reichel's (1975) analysis, with two major modifications. First, to balance the water budget over the oceanic model domain, all the freshwater flux beyond 64°N/S is assumed to concentrate in the northern/southern boundary region. Second, we average the freshwater flux profiles between the two hemispheres, and approximate it by Legendre polynomials, which are antisymmetric about the equator. Consequently, the freshwater is conserved within each hemisphere, and no moisture transport crosses the equator. The resulting meridional freshwater flux, F_w, is shown in Fig. 4. Note that F_w is the total moisture flux, not the flux per unit area. There is no zonal moisture flux in our model.

Since we wish to explore how our ocean GCM responds to changes in the strength of the hydrological cycle, we introduce a factor, μ, which multiples the observationally based moisture flux, F_w, to give the atmospheric meridional moisture flux in a given experiment, μF_w. Then the surface flux of moisture into the ocean is simply taken to be the convergence of the moisture flux over the ocean. Since the ratio of ocean area to total area at each latitude in our model is 1:3 (except in the ACC), the total flux of moisture into the ocean is given by $(\mu/3)$ divF_w (except in the ACC), and is assumed to be zonally uniform. Values of $\mu > 1$ can also be thought of as corresponding to runoff from the land into the ocean supplementing the observed moisture flux over the ocean where precipitation exceeds evaporation, although where evaporation exceeds precipitation it would have to correspond to an enhanced evaporation. However we will also include in our study values of $\mu < 1$, so as to explore fully the sensitivity of the solutions to the strength of the hydrological cycle.

3. Conveyor belt circulation equilibrium response to changes in hydrological cycle

a. Spinup procedure

The model spins up from a motionless state with horizontally uniform temperature and salinity distributions. The initial temperature is taken from the observed globally averaged vertical profile (Levitus 1982), and the initial salinity is set to 34.2 ppt at all levels. The spinup procedure to obtain the conveyor belt circulation is, in most aspects, identical to that used in MW91 and can be divided into three stages.

1) STAGE I

For the first 1000 yr of integration, restoring conditions for surface temperature and salinity are used. The

surface temperature is restored to the T^* profile with a timescale of 288 days, as discussed in section 2b. The surface salinity is restored to an idealized salinity profile, with a timescale of 30 days. The idealized salinity profile is taken from MW91. This restoring stage ensures that the surface salinity field is spun up quickly.

2) STAGE II

In this stage, the salinity condition is switched to a fixed freshwater flux derived from the observed atmospheric moisture transport (e.g., $\mu = 1.5$), whereas the temperature condition remains the same as in stage I. These mixed boundary conditions are used during the rest of the procedure (stages II and III).

At the end of stage I, deep water is forming in the northern oceans of both basins. To establish a state with deep water formation in the North Atlantic only, that is, a ''conveyor belt'' circulation, the freshwater flux is perturbed by ± 0.9 m yr^{-1} north of 40°N, in the Pacific and Atlantic basins, respectively. Thus there is a specified, temporary zonal atmospheric freshwater transport from the Atlantic to the Pacific. The perturbation lasts for 2000 yr, until the conveyor belt circulation is fully set up. Then the perturbation is switched off, marking the end of stage II.

3) STAGE III

To allow the conveyor belt circulation to reach equilibrium, the integration is continued for another 3000 yr after the perturbation has been switched off.

b. Control run

The equilibrium state at the end of stage III, when $\mu = 1.5$, has a NADW formation rate of 18 $\pm$ 1 Sv near 48°N, and there is no deep water formed in the North Pacific (Fig. 5). In comparison, the estimated NADW formation based on observations is 27 $\pm$ 3 Sv near 48°N (Macdonald and Wunsch 1996). Across 25°N, the North Atlantic overturning is estimated to be 17 $\pm$ 3 Sv by Macdonald and Wunsch (1996), whereas the model reaches about 10 Sv. As will be seen in the following discussion, the NADW formation rate increases with μ. We could tune that factor to achieve a stronger overturning that is close to the observed value, but when μ is made that strong the overturning state is unstable in the fully coupled version of our model (Part II). Therefore, the multiplicative factor of 1.5 was chosen for our control run. This corresponds to the observed moisture flux with a moderate amount of runoff from land. Other model parameters (such as vertical diffusivity) could also be tuned to obtain a more realistic NADW formation rate. However, we deemed this unnecessary for a process model study like ours.

Despite its relatively weak overturning strength, the simulated conveyor belt circulation in the model captures some realistic features that are generally missing when mixed boundary conditions with a conventional relaxation time are used. For example, the SST north of 48°N in the Atlantic is up to 9°C warmer than that in the Pacific (Fig. 6), since the deep water formation in the North Atlantic leads to more warm water advection from low latitudes. Such an interbasin SST difference is not captured if the temperature restoring time is too short (e.g., 30 days used in the conventional mixed boundary conditions).

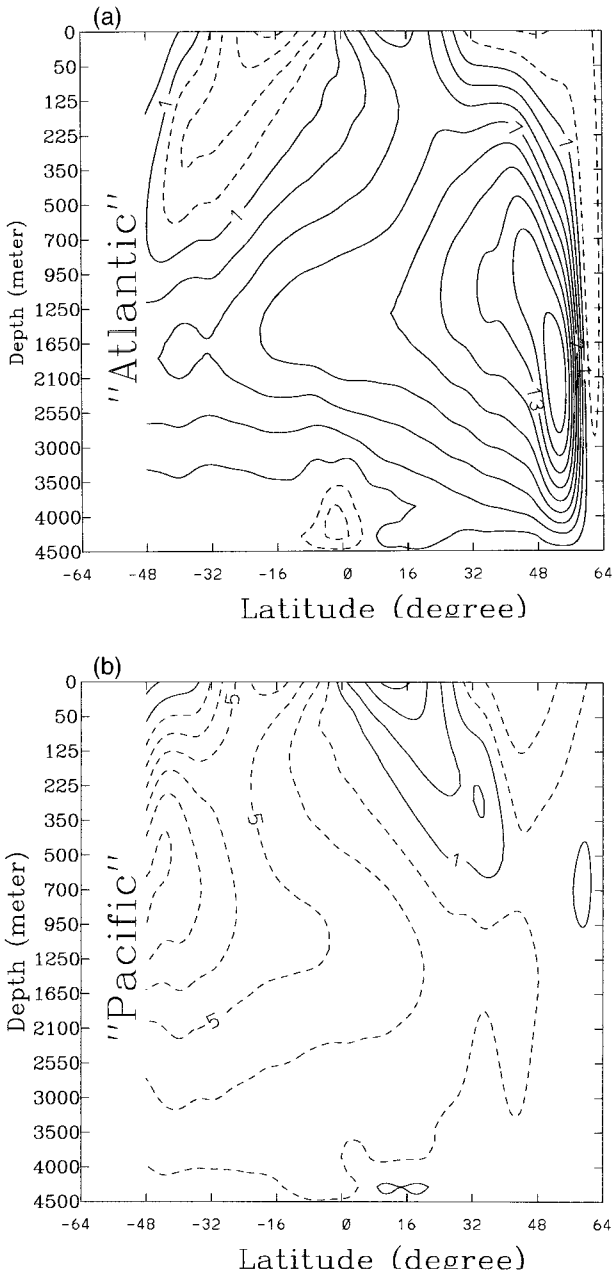

FIG. 5. The control run with $\mu = 1.5$: meridional overturning streamfunction (in Sv): Atlantic (top) and Pacific (bottom). Contour interval: 2 Sv.

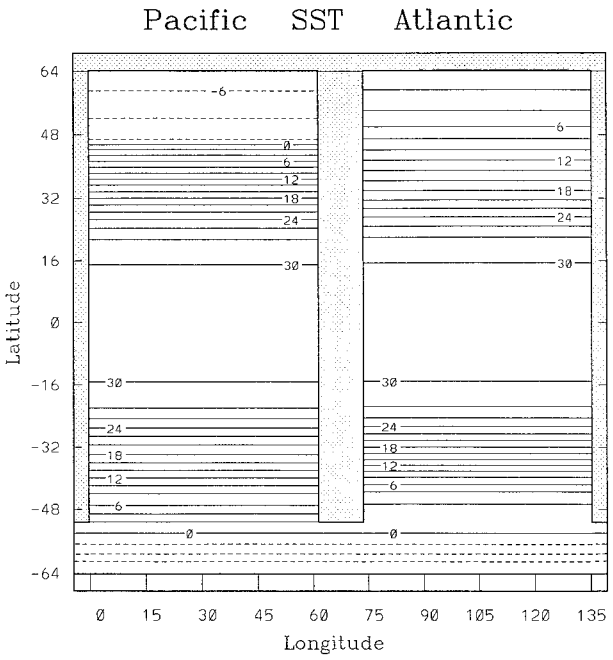

FIG. 6. The SST (°C) distribution at the equilibrium state of the control run for the conveyor belt circulation. Contour interval: 2°C.

c. *Conveyor belt circulation under different hydrological cycles*

A set of experiments with different multiplicative factors $\mu = 0.5$, 1.0, 1.5, and 3.0 were carried out to explore the sensitivity of the circulation to the hydrological cycle. The case $\mu = 1.5$ corresponds to the control run of the last section. The same spinup procedure, described in section 3a, is applied in each experiment. All the runs achieve a stable conveyor belt circulation at the end of the integrations. The North Atlantic overturning intensity increases as the oceanic freshwater flux increases. The case $\mu = 3.0$ has the strongest overturning in the North Atlantic, 28 Sv, whereas the case $\mu = 0.5$ has the weakest overturning, 12 Sv. The result that the conveyor belt circulation is stronger under a stronger freshwater flux is counterintuitive, since enhanced freshening in high latitudes of the North Atlantic is expected to reduce the NADW formation, and therefore, to weaken the overturning, as evidenced by the global warming experiments of Manabe and Stouffer (1994).

The apparent contradiction is resolved if we note the existence of multiple equilibria of the thermohaline circulation. What we found is actually the *conveyor belt* equilibrium corresponding to different freshwater fluxes, whereas Manabe and Stouffer (1994) found a transition to the southern sinking equilibrium. It is also easy to switch to the southern sinking state in our model by simply changing the initial state of the thermohaline circulation. The switching between different equilibria will be studied in the next section.

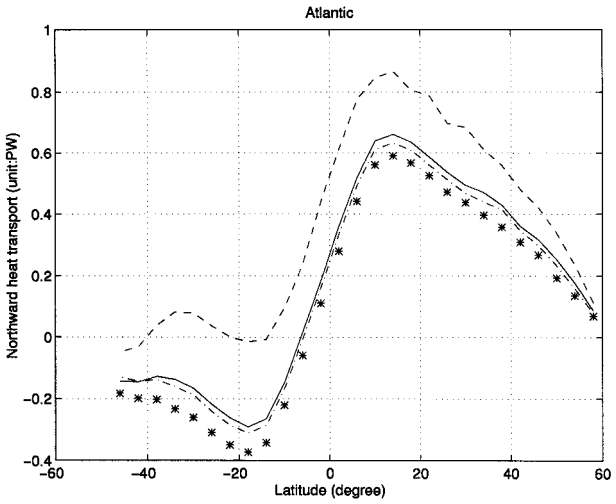

FIG. 7. The Atlantic latitudinal distributions of the northward oceanic heat transports (in PW) when $\mu = 3.0$ (dashed), 1.5 (solid), 1.0 (dash-dotted), and 0.5 (starred).

Note that we compare the thermohaline circulation *equilibrium* responses within the same category (i.e., the conveyor belt type). Figure 7 shows the northward oceanic heat transports in the Atlantic basin for different values of μ. In all four cases the poleward transport is greater in the Northern Hemisphere than in the Southern Hemisphere, but the dominance of the Northern Hemisphere increases as μ and the strength of the Atlantic overturning increase. Another interesting diagnostic, following Walin (1982) and Speer and Tziperman (1992), is the surface density flux. In a purely dynamical context, one need not distinguish the heat and freshwater fluxes, but combine the two into the surface density flux, defined as

$$F_\rho = -\rho(\alpha F_T - \beta F_S), \tag{5}$$

where F_T is surface temperature flux, F_S is implied surface salt flux, and ρ is density. The latitudinal distributions of the Atlantic surface density flux are compared in Fig. 8 for the different values of μ. As shown, the surface density fluxes in the North Atlantic north of 50°N are actually very close, even though their temperature and haline components are quite different. In effect, the increased surface moisture flux into the northern North Atlantic is offset by the increased surface heat flux out of the northern North Atlantic. In contrast, in the South Atlantic, the surface density fluxes are significantly different, because there is too little flux of heat out of the South Atlantic in high latitudes to compensate for the changes in the moisture flux.

Figure 9 shows the northward ocean heat transport in the Pacific basin for different values of μ. For the smaller values of μ (0.5, 1.0, 1.5) the northward heat transport decreases, just the opposite of the behavior in the Atlantic. For these values of μ the changes in the two basins are relatively small and tend to compensate

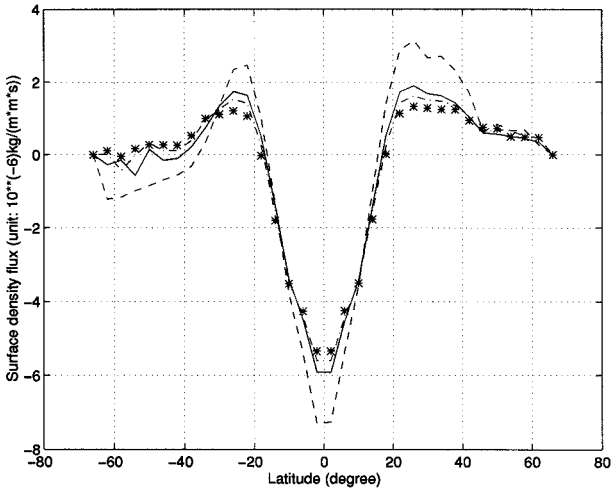

FIG. 8. The Atlantic latitudinal distributions of the surface density fluxes in the steady states with $\mu = 3.0$ (dashed), $\mu = 1.5$ (solid), $\mu = 1.0$ (dash-dotted), and $\mu = 0.5$ (starred); unit: 10^{-6} kg m^2 s^{-1}.

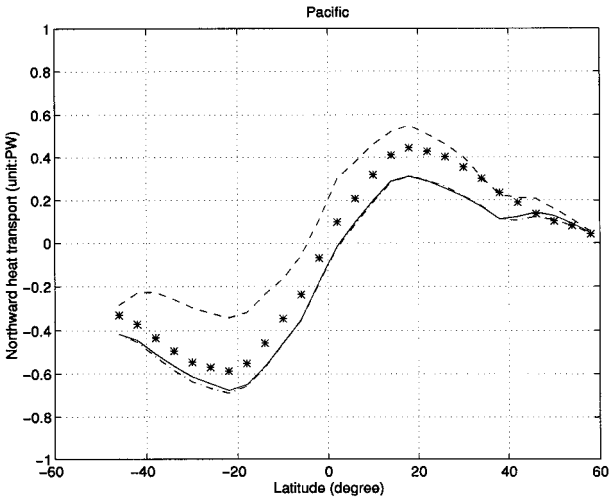

FIG. 9. Same as Fig. 7 but for the Pacific basin.

each other. Indeed, the total Atlantic plus Pacific transport is almost identical for these three cases (differences ≤ 0.1 PW), consistent with what one would expect from heat balance considerations alone, when there is no change in the thermal forcing (Stone 1978). However when $\mu = 3.0$, the strong freshwater flux into the southern high-latitude ocean is sufficient to cause the Southern Ocean Deep Water (SODW) formation to be shut off (see Fig. 11 below), the southern Pacific thermohaline circulation and its associated southward heat transport collapse, and the northward heat transport in the Pacific and globally increase substantially (by about 0.6 PW globally).

The result that changes in the atmospheric freshwater flux influence the equilibrium state primarily through changes in the flux in the Southern Hemisphere is consistent with the simple three-box model of Rooth (1982), who conceptualized the thermohaline circulation as a pole-to-pole deep circulation. He parameterized the flow strength as a linear function of the density difference between the two high-latitude boxes. He found that the steady-state flow strength increases with the freshwater flux intensity. Assuming that the temperature was symmetric about the equator, he showed that the flow strength ϕ follows a square root dependence on the freshwater flux intensity,

$$\phi \propto \sqrt{\mu F_w}. \tag{6}$$

The high-latitude salinity and hence density in the hemisphere with sinking is little influenced by changing μ, because the globally averaged salinity, which is independent of μ, is approximately equal to the globally averaged salinity below the thermocline, which in turn is nearly identical to the surface salinity of the deepwater formation site (Klinger and Marotzke 1999). On the other hand, the high-latitude density in the hemisphere with rising is directly influenced by the change in μ, and decreases as μ increases. As a result, buoyancy increases in the rising hemisphere, and the steady-state flow intensity increases as μ increases.

The GCM results are compared directly to the square-root law prediction in Fig. 10, which shows that in both cases the overturning increases with Fw. However, we note that the apparent good agreement between the two models breaks down as μ goes to zero. For the extreme case of no freshwater flux, the GCM cannot maintain a conveyor belt circulation because there is no salinity gradient to sustain the asymmetry between the two basins. Thus, although Rooth's model captures the qualitative behavior of the Atlantic basin over part of parameter space, it cannot model all the behavior of a two-basin model.

The interhemispheric dynamics analyses in Rooth

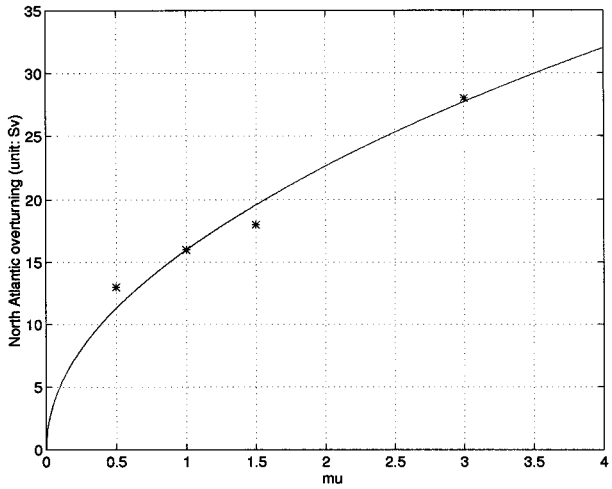

FIG. 10. North Atlantic overturning strength vs the global hydrologic cycle strength: the square-root law prediction fitted to the GCM result for $\mu = 1$ (solid curve), and the GCM results for various values of μ (asterisks).

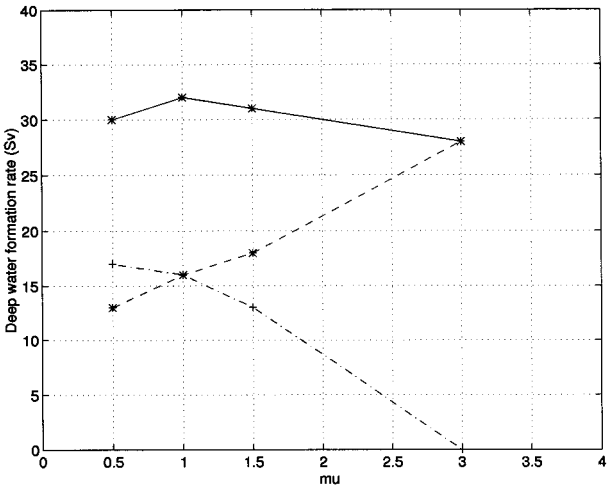

FIG. 11. The equilibrium formation rate of NADW (dashed), SODW (dash-dotted), and their sum (solid), as functions of μ.

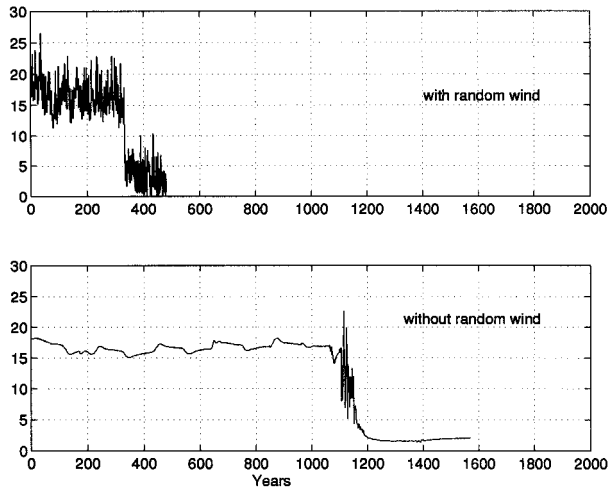

FIG. 12. Time series of the North Atlantic overturning strength (vertical axis in Sv), as μ_N increases. The top panel is with the random wind stress variations, while the bottom is without.

(1982) have been extended by Rahmstorf (1996) and Scott et al. (1999). They found that only the freshwater flux in the Southern Hemisphere appears in the square root relation—that is, ϕ is independent of the moisture flux in the Northern Hemisphere.

Another interesting question is what controls the global deep water formation, which is defined as the sum of NADW formation and SODW formation. Figure 11 shows the NADW and SODW formation rates, and their sum, as a function of the surface freshwater fluxes. Although the two parts of the global deep water formation rates are very sensitive to the freshwater fluxes, their sum is only weakly influenced. This indicates that Rooth's pole-to-pole picture is not directly related to the global deep water formation, but only to the NADW branch of the global conveyor belt circulation—another limitation of Rooth's model. However, the *global* deep water formation in a single basin model is not sensitive to the freshwater flux (Klinger and Marotzke 1998), and our result suggests that this is also true for a two-basin model. On the other hand, Fig. 11 implies that the freshwater flux plays a crucial role in partitioning the deep water formation rates between the north and the south.

4. Conveyor belt circulation transient responses to hydrological cycle changes

a. Perturbation method

Motivated by the results of global warming scenarios in coupled GCMs (e.g., Manabe and Stouffer 1994), we next look at our model's transient response to gradual changes in the atmosphere's hydrological cycle. We perturb the amplitude of the freshwater flux in each hemisphere separately and jointly, in order to distinguish the roles of the two hemispheres. The equilibrium state to which we apply the perturbation is the steady state from the control run in the last section, with $\mu = 1.5$. Since the atmospheric moisture fluxes in the Northern and Southern Hemispheres are not always the same in these experiments, we now distinguish two multiplicative factors, μ_N and μ_S, which multiply F_w in the Northern and Southern Hemispheres, respectively. In these experiments μ_N or μ_S or both of them are increased linearly by 1.5×10^{-3} yr^{-1} (0.1% of the initial value). To follow the response of the conveyor belt circulation, we monitor the maximum value of the zonal-mean mass transport streamfunction below 950-m depth in the North Atlantic (to exclude the Ekman layer). In effect, this is our definition of the strength of the North Atlantic overturning circulation.

In these experiments we also include random variations in the zonal wind stress field north of 46°N. The variations are uniform in space and have a Gaussian distribution, with zero mean and standard deviation of 1 dyn cm^{-2}, based on European Centre for Medium-Range Weather Forecasts (ECMWF) analyses (D. Stammer 1996, personal communication). Our motivation in applying these random variations in wind stress is illustrated by two experiments, one with random wind variations, the other without, in which μ_N increases according to the above prescription. Figure 12 shows the time series of the North Atlantic overturning strength in these two experiments. The random wind variations give rise to interannual variations in the strength of the overturning, which are comparable in magnitude to those found in experiments with coupled GCMs (e.g., Manabe and Stouffer 1994), whereas interannual variations are almost absent without them.

The variations also accelerate the collapse of the overturning, therefore speeding up the response time of the model to the freshwater flux perturbation (see Fig. 12). The reason for the acceleration of the collapse is that the variations make it harder for the convection to sustain itself. The convection tends to maintain itself, be-

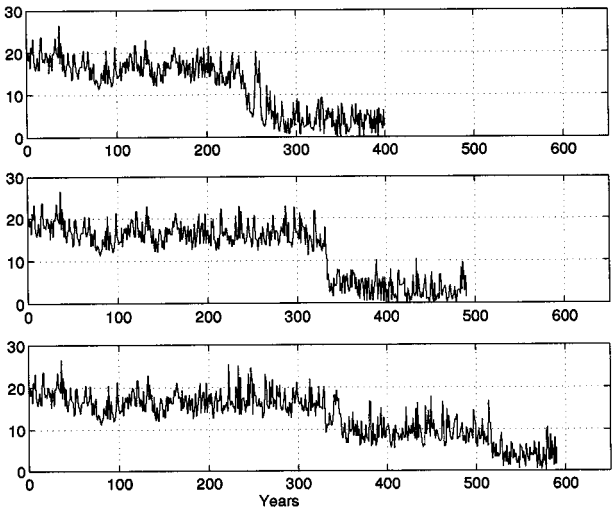

FIG. 13. Time series of the maximum North Atlantic overturning strength (vertical axis in Sv), when the wind stress variations are calculated with three different initial random seeds, and μ_N increases linearly.

cause of a positive feedback with the overturning circulation (Lenderink and Haarsma 1994). Once the convection is triggered, it creates favorable conditions for further convection there. This positive feedback is so powerful that in the case without random variations the convection does not shut off until the freshening is virtually doubled at the convection site (around year 1000). When the random variations are present, they generate perturbations in the Ekman currents, which are propagated downward to the deep layers, and cause variations in the overturning strength. This weakens the positive feedback. In general, the random wind stress variations lead to a more realistic variability in the convection sites, and in the strength of the overturning circulation. We note that, even though the transitions are speeded up by the technique, the character of the model behavior is not fundamentally altered by including the random wind variations.

Another question that is relevant with the random stress variations is whether the overturning behavior is sensitive to the choice of the initial random seed in the calculation. This question is pertinent to the predictability of the evolution of the thermohaline circulation. Figure 13 shows the evolution of the North Atlantic overturning strength for three runs in which μ_N increases as in the previous experiments, but three different choices are made for the initial random seed. (The second of these is the same experiment shown in the top of Fig. 12.) The results shown in Fig. 13 suggest that the predictability of the overturning is limited to about the first 200 yr of its evolution. This behavior is of great interest, but will not be pursued further in this paper. To exclude the effect of different initial conditions, all the experiments in this section use the *identical initial random seed* to calculate the random wind stress variations.

b. Increasing hydrological cycle in the Northern Hemisphere

As the freshwater flux in the Northern Hemisphere (μ_N) increases linearly, the overturning remains essentially unchanged until it suddenly collapses to a state with sinking in the Southern Ocean (Fig. 13, top). The collapse occurs at about year 270, when μ_N has increased about 27%. A similar collapse was found in the global warming experiments of Manabe and Stouffer (1994). In those experiments the atmospheric moisture transport became stronger due to warming, and the enhanced freshening in high latitudes resulted in the weakening/collapsing of the thermohaline circulation. Assuming that this moisture transport increase in the global warming experiments was due to the increasing moisture capacity of the atmosphere, as suggested by Manabe and Stouffer (1994), we estimate from the Clausius–Clapeyron equation that the transport in the Northern Hemisphere in those experiments increased about six times more rapidly than in our experiment. This much more rapid increase may explain why the overturning steadily declined over the first 200 yr of the global warming experiments, whereas it does not in our experiment. Also we note that the warming in the global warming experiments was much greater in middle and high latitudes of the Northern Hemisphere than in the Southern Hemisphere. Thus our experiment with μ_N increasing is a much closer analog of the global warming experiments than the experiments described below, in which only μ_S increases, or in which μ_S and μ_N increase at the same rate.

To examine whether the collapse in our experiment represents a transition from a stable regime to an unstable regime, we apply to the collapsed state the same freshwater flux perturbation as that used in stage II of the spinup procedure, so as to reestablish the conveyor belt state. With μ_N fixed at 2.0 and μ_S at 1.5, the conveyor belt state is successfully reestablished, with the formation rate for NADW similar to that of the overturning before the collapse. Furthermore, the reestablished conveyor belt state is stable. This result demonstrates that the transition need not be permanent, rather, the overturning collapse depends on the evolution of the perturbation applied.

c. Increasing hydrological cycle in the Southern Hemisphere

In this experiment μ_S increased linearly at the rate of 1.5×10^{-3} yr^{-1}. In response to the perturbation, the North Atlantic overturning increases gradually with time, consistent with the equilibrium changes found in section 3, but at quite a small rate (Fig. 14). This slow response indicates a long delay in the response of the

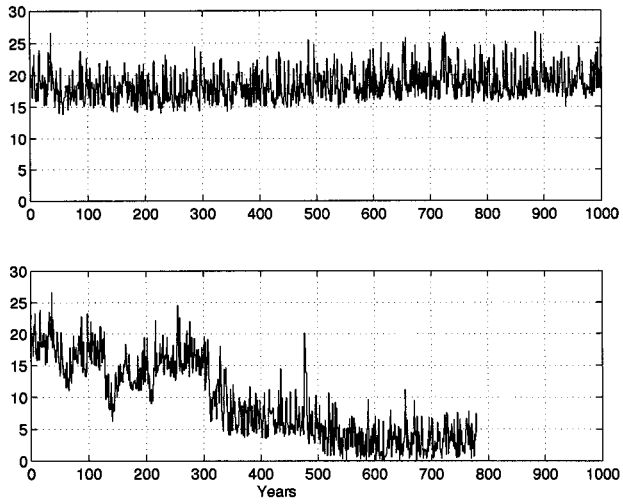

FIG. 14. Time series of the North Atlantic overturning strength (vertical axis in Sv), as (top) μ_S increases linearly; and (bottom) as both μ_N and μ_S increase linearly.

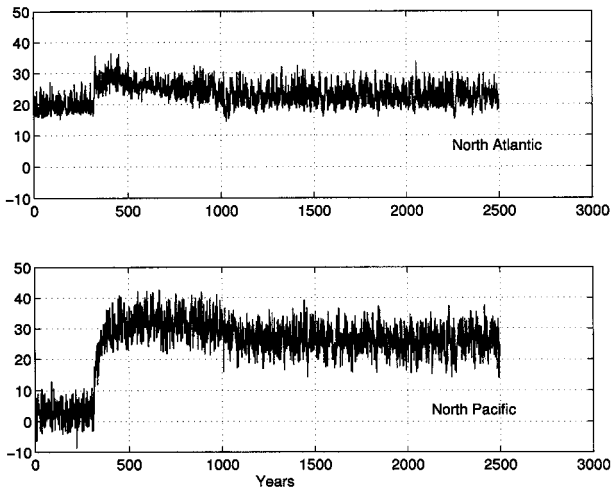

FIG. 15. Time series of the overturning strength (vertical axis in Sv) (top) in the North Atlantic, and (bottom) in the North Pacific, under fixed forcing with $\mu_S = 3.0$ and $\mu_N = 1.5$, starting from the final state of Fig. 14 (top).

North Atlantic overturning to changes in the Southern Hemisphere, consistent with the advection timescale from the South Ocean to the North Atlantic sinking region being more than several hundred years. The state at the end of the perturbation (year 1000) has not yet reached equilibrium. To demonstrate this, the forcing after 1000 yr is held fixed, with $\mu_N = 3.0$ and $\mu_S = 1.5$, and another 2500 yr of integration is carried out, until the equilibrium state is reached. Figure 15 displays the time series of the overturnings in the North Atlantic and North Pacific for these last 2500 yr. At about year 350, the conveyor belt state switches to a northern sinking state, with sinking in both ocean basins. The steady sinking strengths of the two basins are close to each other, and are about 24 Sv in each basin.

d. Increasing hydrological cycle in both hemispheres

In this experiment, both μ_N and μ_S increase at the rate of 1.5×10^{-3} yr^{-1}. The result is shown in the bottom panel of Fig. 14. In this case the interannual variability is much greater than when only μ_N or μ_S increases, a temporary weakening and a partial collapse of the thermohaline circulation set in earlier (after 140 yr) than in the case with only μ_N increasing (top panel of Fig. 13), but the complete collapse is delayed. Although μ_S dominates the steady-state overturning strength, it does not obviously stabilize NADW formation against increased Northern Hemisphere freshwater forcing.

5. Summary and discussion

The sensitivity of the thermohaline circulation to changes of the surface freshwater fluxes has been systematically investigated in an idealized global OGCM combined with a simple atmospheric model based on observed transports of heat and moisture. We find that the North Atlantic Deep Water (NADW) formation rate at equilibrium increases as the global freshwater fluxes in the atmosphere increase. Following the reasoning of Manabe and Stouffer (1994), who argued that the collapse of the North Atlantic overturning in their global warming experiment with a coupled GCM was caused by the increase of atmospheric moisture transport in the warmer climate, we had expected the stronger freshwater flux to lead to a weaker overturning. In fact, Manabe and Stouffer's reasoning applies only to the Northern Hemisphere, where the increased freshwater flux tends to reduce the sinking that forms the deep water, thus reducing the overturning strength. In the Southern Hemisphere where the overturning is rising rather than sinking, the effect is the opposite, and in our model this effect dominates. This result illustrates that changes in the thermohaline circulation can be predicted correctly only in models that simulate the hemispheric asymmetries accurately.

Although the NADW formation rate is sensitive to the freshwater flux, the global deep water formation rate—that is, the sum of the NADW and the Southern Ocean Deep Water formation rates—is relatively insensitive to the freshwater fluxes. Other studies suggest that the global deep water formation is sensitive to the value of vertical diffusivity in the OGCM (Bryan 1987; Marotzke 1997) and to the pole-to-equator temperature difference (Marotzke 1997; Klinger and Marotzke 1999). Also, Tziperman (1997) found that even though the NADW formation rate is sensitive to the restoring surface salinity profile in northern high latitudes, the global deep water formation rate remained less sensitive to such changes. However, what is new from our study is that the magnitude of the global freshwater flux governs

the partitioning of deep water formation between the North Atlantic and the Southern Ocean.

When the freshwater flux increases, whether separately in each hemisphere or jointly, all our results are consistent with the suggestion (Rahmstorf 1996; Scott et al. 1999) that, for realistic parameter values, the equilibrated response of the overturning is governed primarily by the freshwater flux in the Southern Hemisphere. The freshwater flux in the Northern Hemisphere seems to have surprisingly little control on the equilibrium state of the overturning. This can be explained by the fact that surface salinity in the deep convection region, from where most of the ocean volume is ventilated, is closely tied to the (constant) global average salinity, whereas surface salinity in the upwelling high latitudes is influenced by the strength of the freshwater flux. Such an asymmetric role of the two hemispheres' freshwater fluxes is also found in Rooth's box model (Rahmstorf 1996; Scott et al. 1999).

Our results also indicate that the stability of the North Atlantic overturning is affected by two processes. First is the freshwater input over high-latitude convection sites; sufficient freshening can shut off the North Atlantic Deep Water formation. Manabe and Stouffer (1994) attributed the collapse of the North Atlantic overturning in their global warming experiments to an increase in this freshening. On the other hand, Scott et al. (1999) found, using Rooth's box model, that increasing the ratio of the freshwater fluxes in the two hemispheres (north vs south) destabilizes the large-scale thermohaline circulation. Although our model's stability characteristics are much more complicated than those of the Rooth model, we have nevertheless found a qualitatively similar behavior—that is, the stability characteristics of the North Atlantic overturning circulation depend on the asymmetry of the moisture flux in the two hemispheres. In particular, stronger fluxes in the Southern Hemisphere favor greater stability in the North Atlantic. This suggests again that simulations of changes in the thermohaline circulation caused by global warming need an accurate simulation of the hemispheric asymmetry in the warming. This result, along with our results for the dependence of the strength of the North Atlantic overturning on the moisture flux in the Southern Hemisphere, clearly indicate that hemispheric models of the thermohaline circulation have limited realism.

Finally, our experiments have shown that the evolution of the thermohaline circulation can be sensitive to the atmospheric initial conditions. This behavior needs to be studied in much greater detail, and with models as realistic as possible, in order to determine the predictability of the climate state.

Acknowledgments. We are indebted to Jeffery Scott for many useful discussions and comments. Sixty percent ($46,000) of this research was funded jointly by the U.S. Department of Energy's (DoE) National Institute for Global Environmental Change (NIGEC) through the NIGEC Northeast Regional Center at Harvard University (DoE Cooperative Agreement DE-FC03-90ER61010) and by the DoE's Program for Computer Hardware, Applied Mathematics, and Model Physics. Financial support was also contributed by the Tokyo Electric Power Company (TEPCO) through the TEPCO/MIT Environmental Research Program and by the Massachusetts Institute of Technology Joint Program (JP) on the Science and Policy of Global Change. Financial support does not constitute an endorsement by DoE, TEPCO, or the JP of the views expressed in this article.

REFERENCES

Baumgartner, A., and E. Reichel, 1975: *The World Water Balance.* Oldenbourg Verlag, 179 pp.

Broecker, W. S., M. Andree, W. Wolli, H. Oeschger, G. Bonani, J. Kennett, and D. Peteet, 1988: A case in support of a meltwater diversion as the trigger for the onset of the Younger Dryas. *Paleoceanography,* **3,** 1–19.

Bryan, F., 1987: Parameter sensitivity of primitive equation ocean general circulation models. *J. Phys. Oceanogr.,* **17,** 970–985.

Bryan, K., 1984: Accelerating the convergence to equilibrium of ocean-climate models. *J. Phys. Oceanogr.,* **14,** 666–673.

——, S. Manabe, and R. Pacanowski, 1975: A global ocean-atmosphere climate model. Part II: The oceanic circulation. *J. Phys. Oceanogr.,* **5,** 30–46.

Budyko, M. I., 1969: The effect of solar radiation variations on the climate of the earth. *Tellus,* **21,** 611–619.

Chen, F., and M. Ghil, 1995: Interdecadal variability of the thermohaline circulation and high-latitude surface fluxes. *J. Phys. Oceanogr.,* **25,** 2547–2568.

Haney, R. L., 1971: Surface thermal boundary conditions for ocean circulation models. *J. Phys. Oceanogr.,* **1,** 241–248.

Huang, R. X., and R. L. Chou, 1994: Parameter sensitivity study of the saline circulation. *Climate Dyn.,* **9,** 391–409.

Hughes, T., and A. J. Weaver, 1994: Multiple equilibria of an asymmetric two-basin model. *J. Phys. Oceanogr.,* **24,** 619–637.

Keith, D., 1995: Meridional energy transport: Uncertainty in zonal means. *Tellus,* **47A,** 30–44.

Klinger, B. A., and J. Marotzke, 1999: Behavior of double hemisphere thermohaline flows in a single basin. *J. Phys. Oceanogr.,* in press.

Lenderink, G., and R. J. Haarsma, 1994: Variability and multiple equilibria of the thermohaline circulation associated with deep water formation. *J. Phys. Oceanogr.,* **24,** 1480–1493.

Levitus, S., 1982: *Climatological Atlas of the World Ocean.* NOAA Professional Paper 13, U.S. Dept. of Commerce, NOAA, Washington, DC, 173 pp.

Macdonald, A., and C. Wunsch, 1996: An estimate of global ocean circulation and heat fluxes. *Nature,* **382,** 436–439.

Manabe, S., and R. Stouffer, 1994: Multiple-century response of a coupled ocean-atmosphere model to an increase of atmospheric carbon dioxide. *J. Climate,* **7,** 5–23.

Marotzke, J., 1997: Boundary mixing and the dynamics of three-dimensional thermohaline circulations. *J. Phys. Oceanogr.,* **27,** 1713–1728.

——, and J. Willebrand, 1991: Multiple equilibria of the global thermohaline circulation. *J. Phys. Oceanogr.,* **21,** 1372–1385.

——, and P. H. Stone, 1995: Atmospheric transports, the thermohaline circulation, and flux adjustments in a simple coupled model. *J. Phys. Oceanogr.,* **25,** 1350–1364.

North, G. R., 1975: Theory of energy-balance climate models. *J. Atmos. Sci.,* **32,** 2033–2043.

Oort, A. H., 1983: Global atmospheric circulation statistics, 1958–73. NOAA Prof. Paper No. 14, U.S. Dept. of Commerce, Washington, DC, 180 pp.

Pacanowski, R. C., K. Dixon, and A. Rosati, 1991: The GFDL Modular Ocean Model Users Guide. Version 1.0, GFDL Ocean Group Tech. Rep. 2, 376 pp. [Available from GFDL, Box 308, Route 1, Princeton, NJ 08542.]

Rahmstorf, S., 1996: On the freshwater forcing and transport of the Atlantic thermohaline circulation. *Climate Dyn.,* **12,** 799–811.

Rooth, C., 1982: Hydrology and ocean circulation. *Progress in Oceanography,* Vol. 11, Pergamon Press, 131–149.

Schopf, P. S., 1983: On equatorial waves and El Niño. Part II: Effects of air–sea thermal coupling. *J. Phys. Oceanogr.,* **13,** 1878–1893.

Scott, J., P. H. Stone, and J. Marotzke, 1999: Interhemispheric thermohaline circulation in a coupled box model. *J. Phys. Oceanogr.,* in press.

Speer, K., and E. Tziperman, 1992: Rates of water mass formation in the North Atlantic Ocean. *J. Phys. Oceanogr.,* **22,** 93–104.

Stephens, G. L., G. G. Campbell, and T. H. Vonder Haar, 1981: Earth radiation budgets. *J. Geophys. Res.,* **86,** 9739–9760.

Stone, P. H., 1978: Constraints on dynamical transports of energy on a spherical planet. *Dyn. Atmos. Oceans,* **2,** 123–139.

Trenberth, K. E., and A. Solomon, 1994: The global heat balance: Heat transports in the atmosphere and ocean. *Climate Dyn.,* **10,** 107–134.

Tziperman, E., 1997: Inherently unstable climate behavior due to weak thermohaline ocean circulation. *Nature,* **386,** 592–595.

Walin, G., 1982: On the relation between sea-surface heat flow and thermal circulation in the ocean. *Tellus,* **34,** 187–195.

Wang, X., P. H. Stone, and J. Marotzke, 1998: Global thermohaline circulation. Part II: Sensitivity with interactive atmospheric transports. *J. Climate,* **12,** 83–91.

Weaver, A. J., and E. S. Sarachik, 1990: On the importance of vertical resolution in certain ocean general circulation models. *J. Phys. Oceanogr.,* **20,** 600–609.

——, ——, and J. Marotzke, 1991: Freshwater flux forcing of decadal and interdecadal oceanic variability. *Nature,* **353,** 836–838.

——, J. Marotzke, P. F. Cummins, and E. S. Sarachik, 1993: Stability and variability of the thermohaline circulation. *J. Phys. Oceanogr.,* **23,** 39–60.

Winton, M., and E. S. Sarachik, 1993: Thermohaline oscillations induced by strong steady salinity forcing of ocean general circulation models. *J. Phys. Oceanogr.,* **23,** 1389–1409.

Yin, F. L., and E. S. Sarachik, 1994: An efficient convection adjustment scheme for ocean general circulation models. *J. Phys. Oceanogr.,* **24,** 1425–1430.

Zhang, S., R. J. Greatbatch, and C. A. Lin, 1993: A reexamination of the polar halocline catastrophe and implications for coupled ocean-atmosphere modeling. *J. Phys. Oceanogr.,* **23,** 287–299.